

## Article

# Gradual Replacement of $\text{Ca}^{2+}$ with $\text{Mg}^{2+}$ Ions in Brushite for the Production of $\text{Ca}_{1-x}\text{Mg}_x\text{HPO}_4 \cdot n\text{H}_2\text{O}$ Materials

Mazen Alshaaer <sup>1</sup>, Khalil Issa <sup>2</sup>, Abdulaziz Alanazi <sup>1</sup>, Saida Abu Mallouh <sup>3</sup>, Ahmed S. Afify <sup>4</sup>,  
Moustapha E. Moustapha <sup>5</sup> and Kostas Komnitsas <sup>6,\*</sup>

- <sup>1</sup> Department of Physics, College of Science and Humanities in Al-Kharj, Prince Sattam Bin Abdulaziz University, Al-Kharj 11942, Saudi Arabia; mazen.alshaaer@yahoo.com (M.A.); abdulazizaoda@gmail.com (A.A.)
- <sup>2</sup> Orthopedics Unit, Faculty of Medicine and Health Sciences, An-Najah National University, Nablus 00970, Palestine; k.issa@najah.edu
- <sup>3</sup> Hamdi Mango Center for Scientific Research, The University of Jordan, Amman 11942, Jordan; saida387439@yahoo.com
- <sup>4</sup> Department of Basic Sciences, The Higher Institute of Engineering and Automotive Technology and Energy, New Heliopolis, Cairo 11829, Egypt; Sabry44484@hotmail.com
- <sup>5</sup> Department of Chemistry, College of Science and Humanities in Al-Kharj, Prince Sattam bin Abdulaziz University, Al-Kharj 11942, Saudi Arabia; m.moustapha@psau.edu.sa
- <sup>6</sup> School of Mineral Resources Engineering, Technical University of Crete, 73100 Chania, Greece
- \* Correspondence: komni@mred.tuc.gr; Tel.: +30-28210-37686

**Abstract:** The present study investigates the gradual replacement of  $\text{Ca}^{2+}$  with  $\text{Mg}^{2+}$  ions in brushite ( $\text{CaHPO}_4 \cdot 2\text{H}_2\text{O}$ ). To date, this approach has not been systematically explored and may prove beneficial for the production of  $\text{Ca}_{1-x}\text{Mg}_x\text{HPO}_4 \cdot n\text{H}_2\text{O}$  materials with tailored properties which are suitable for environmental and medical applications. For their production, solutions of sodium dihydrogen orthophosphate dehydrate,  $\text{NaH}_2\text{PO}_4 \cdot 2\text{H}_2\text{O}$ , calcium nitrate tetrahydrate,  $\text{Ca}(\text{NO}_3)_2 \cdot 4\text{H}_2\text{O}$ , magnesium nitrate hexahydrate,  $\text{Mg}(\text{NO}_3)_2 \cdot 6\text{H}_2\text{O}$  and ammonium hydroxide solution,  $\text{NH}_4\text{OH}$ , were used. At low  $\text{Mg}/\text{Ca}$  molar ratios (up to 0.25) in the starting solution, partial replacement of  $\text{Ca}$  with  $\text{Mg}$  takes place ( $\text{Mg}$  doping) but no struvite is produced as discrete phase. When the  $\text{Mg}/\text{Ca}$  molar ratio increases gradually to 1.5, in addition to  $\text{Mg}$ -doped brushite, struvite,  $\text{NH}_4\text{MgPO}_4 \cdot 6\text{H}_2\text{O}$ , precipitates. The microstructure of the materials produced for different degrees of  $\text{Ca}$  replacement with  $\text{Mg}$  has been analyzed in depth with the use of powdered XRD (X-ray diffraction), XPS (X-ray photoelectron spectroscopy), thermogravimetric (TG) analysis and SEM (scanning electron microscopy). The results of this study prove that the  $\text{Mg}/\text{Ca}$  ratio in the starting solution can be monitored in such a way that materials with tailored composition are obtained.

**Keywords:** brushite; struvite; biomaterials; XPS; crystal growth



**Citation:** Alshaaer, M.; Issa, K.; Alanazi, A.; Mallouh, S.A.; Afify, A.S.; Moustapha, M.E.; Komnitsas, K. Gradual Replacement of  $\text{Ca}^{2+}$  with  $\text{Mg}^{2+}$  Ions in Brushite for the Production of  $\text{Ca}_{1-x}\text{Mg}_x\text{HPO}_4 \cdot n\text{H}_2\text{O}$  Materials. *Minerals* **2021**, *11*, 284. <https://doi.org/10.3390/min11030284>

Academic Editor: Felix Brandt

Received: 8 February 2021

Accepted: 7 March 2021

Published: 10 March 2021

**Publisher's Note:** MDPI stays neutral with regard to jurisdictional claims in published maps and institutional affiliations.



**Copyright:** © 2021 by the authors. Licensee MDPI, Basel, Switzerland. This article is an open access article distributed under the terms and conditions of the Creative Commons Attribution (CC BY) license (<https://creativecommons.org/licenses/by/4.0/>).

## 1. Introduction

Calcium phosphates (CaPs) are useful in a variety of medical, environmental, and engineering applications. Since their mineralogical structure and biochemical properties are similar to the mineral phases present in bone tissues, they can substitute bone in medical applications [1,2]. Due to their low toxicity, high bioactivity and excellent biocompatibility, CaP-based biomaterials, biocements and bioceramics exhibit high potential for applications in the fields of medicine, advanced materials and technology [3,4]. They may be used in various forms as self-supported scaffolds, granules with varying porosity, composite materials, injectable bone cements and coatings on dental or hip implants [5,6]. In addition to the medical and pharmaceutical applications, CaPs have been used for a very long period for the production of various types of commercial fertilizers [7] and can be also utilized with the synergistic action of other additives for the production of construction materials or chemically bonded ceramics [8–10].

Brushite (dicalcium phosphate dihydrate (DCPD,  $\text{CaHPO}_4 \cdot 2\text{H}_2\text{O}$ ) is one of the most known CaPs [11] which is stable in a weakly acidic environment (pH 4.0–6.5) and low temperature (less than 80 °C) [12,13]. It can be produced under specific temperature and pH range and is usually metastable at physiological conditions, pH  $\sim$  7.4, thus it can be resorbed within relatively short periods and form bone material [14–17].

Brushite cements exhibit faster setting times and higher biocompatibility, bioresorbability and osteoconductivity under physiological conditions compared to apatite cements [18]. Incorporation of bioactive ions can result in the production of biomaterials with superior mechanical properties. It is known that several dopant ions can preferably substitute  $\text{Ca}^{2+}$  ions on certain atomic positions depending on their ionic radii for the relevant coordination with oxygen.  $\text{Mg}^{2+}$  has a smaller ionic radius compared to  $\text{Ca}^{2+}$  (0.720 and 1.00 Å, respectively), thus its incorporation in  $\beta$ -tricalcium phosphate,  $\text{Ca}_3(\text{PO}_4)_2$  ( $\beta$ -TCP) results in a decrease of the lattice parameters  $a$  and  $c$  [19–22]. Furthermore, the Mg-stabilized  $\beta$ -TCPs exhibit higher thermal stability up to 1400 °C, thus the sintering temperature range is broadened and its transformation into the undesirable  $\alpha$ -TCP is avoided [23–25].

In addition, the incorporation of Mg ions in biomedical materials enhances cell growth and proliferation, while it contributes to sustainable bone formation [26,27]. More specifically,  $\text{Mg}^{2+}$  ions promote the osteogenic differentiation of bone marrow mesenchymal stem cells (MSCs) [28] and the osteogenic bioactivity of recombinant human bone morphogenetic protein-2 (rhBMP-2) [29]. On the other hand, modification of implantable scaffolds with Mg and Zn results in enhanced biocompatibility and improves bone regeneration [30]. In earlier studies it has been shown that the co-substitution of  $\text{Sr}^{2+}$  and  $\text{Mg}^{2+}$  in the  $\beta$ -TCP structure reduces significantly the lattice  $a$ - and  $c$ -axis parameters, while the size effect of  $\text{Mg}^{2+}$  is more noticeable compared to  $\text{Sr}^{2+}$  [31].

The field of biomaterials in which CaPs play a major role has achieved a major breakthrough in recent years and is going to advance further in the near future. Both inorganic and polymeric biomaterials are used for the fabrication of biomimetic scaffolds for bone, periodontal tissue regeneration and skeletal muscle engineering [32]. Furthermore, additional research is required so that the produced bioceramics based on TCP, hydroxyapatite (HA), and their composites acquire important properties such as antibacterial, anti-inflammatory and cellular differentiation. More specifically, the development of biomaterials with antibacterial properties is very urgent due to the exponential growth of antibiotic resistant microorganisms and their enormous impact on global public health [33]. New ceramic-polymer composites may be produced by embedding ceramic particles into the polymer matrix and regulating their properties by monitoring the particle size of CaPs and their distribution in the polymer matrix [34]. So, novel and bio-inspired materials need to be designed in the near future which will mimic tissues at micro and nanoscale [35].

The present research study aims to investigate in sufficient depth the crystal morphology, the chemical composition and the mineralogy of the materials produced when different Mg/Ca molar ratios are used in the starting solution. These aspects will prove beneficial during the future synthesis of (bio)materials with tailored properties and specific functions.

## 2. Experimental Methodology

### 2.1. Materials

Sodium dihydrogen orthophosphate dehydrate,  $\text{NaH}_2\text{PO}_4 \cdot 2\text{H}_2\text{O}$ , was purchased from Techno Pharmchem, India, while calcium nitrate tetrahydrate,  $\text{Ca}(\text{NO}_3)_2 \cdot 4\text{H}_2\text{O}$ , magnesium nitrate hexahydrate,  $\text{Mg}(\text{NO}_3)_2 \cdot 6\text{H}_2\text{O}$  and ammonium hydroxide solution,  $\text{NH}_4\text{OH}$ , from LOBA Chemie, India. Distilled water (0.055  $\mu\text{S}/\text{cm}$ ) was prepared using a water purification system (PURELAB Option-Q, ELGA, High Wycombe, UK). Each component was weighed using a digital analytical balance (EX324N, OHAUS, Parsippany, NJ, USA), while stirring was performed with the use of a magnetic stirrer (ISOTEMP, Fisher Scientific, Shanghai, China). Parsippany

## 2.2. Synthesis of $\text{Ca}_{1-x}\text{Mg}_x\text{HPO}_4 \cdot n\text{H}_2\text{O}$

The synthesis of  $\text{Ca}_{1-x}\text{Mg}_x\text{HPO}_4 \cdot n\text{H}_2\text{O}$  compounds was carried out at room temperature based on the Equation (1), using the following solutions, namely  $\text{Na}_2\text{HPO}_4 \cdot 2\text{H}_2\text{O}$ ,  $\text{Ca}(\text{NO}_3)_2 \cdot 4\text{H}_2\text{O}$  and  $\text{Mg}(\text{NO}_3)_2 \cdot 6\text{H}_2\text{O}$  0.5 mol/L. The molar proportions used in each case for the synthesis of  $\text{Ca}_{1-x}\text{Mg}_x\text{HPO}_4 \cdot n\text{H}_2\text{O}$  compounds with different composition are shown in Table 1.



**Table 1.** Molar proportions of  $\text{NaH}_2\text{PO}_4 \cdot 2\text{H}_2\text{O}$ ,  $\text{Ca}(\text{NO}_3)_2 \cdot 4\text{H}_2\text{O}$  and  $\text{Mg}(\text{NO}_3)_2 \cdot 6\text{H}_2\text{O}$  as well as Mg/Ca molar ratios used for the synthesis of  $\text{Ca}_{1-x}\text{Mg}_x \cdot \text{HPO}_4 \cdot n\text{H}_2\text{O}$  compounds.

Product ID	$\text{NaH}_2\text{PO}_4 \cdot 2\text{H}_2\text{O}$	$\text{Ca}(\text{NO}_3)_2 \cdot 4\text{H}_2\text{O}$	$\text{Mg}(\text{NO}_3)_2 \cdot 6\text{H}_2\text{O}$	Mg/Ca Molar Ratio
BM0	1	1	0	0
BM2	1	0.8	0.2	0.25
BM4	1	0.6	0.4	0.67
BM5	1	0.5	0.5	1.0
BM6	1	0.4	0.6	1.5
BM10	1	0	1	-

First, pure brushite, MB0, was produced by dropwise addition of 100 mL  $\text{Ca}(\text{NO}_3)_2 \cdot 4\text{H}_2\text{O}$  solution (flow rate ~2 mL/min), using a glass funnel with a glass stopcock, to the  $\text{Na}_2\text{HPO}_4 \cdot 2\text{H}_2\text{O}$  solution under continuous stirring (stirring speed 450 rpm) until a Ca/P molar ratio of 1.0 was obtained. The new solution was stirred at room temperature for 1 h to enable full homogeneity. The total stirring period prior to filtering was almost two hours. The pH of the final solution was adjusted to slightly acidic values, between 6 and 6.5, using ammonium hydroxide solution (~15 mol/L) in order to enable the production of a white precipitate, which was then vacuum filtered using a Buchner funnel and a qualitative filter paper (45  $\mu\text{m}$ ,  $\varnothing$  12 cm, Double Rings, China). The filter cake was washed three times with de-ionized water and three more times with ethanol to prevent agglomeration [36]. Then, it was placed on a watch glass and dried overnight at 40 °C in an oven (ED53/E2, Binder, Tuttlingen, Germany).

MB2, MB4, MB5 and MB6 compounds were prepared by mixing first the  $\text{Ca}(\text{NO}_3)_2 \cdot 4\text{H}_2\text{O}$  and  $\text{Mg}(\text{NO}_3)_2 \cdot 6\text{H}_2\text{O}$  solutions using the molar ratios shown in Table 1. Then, 100 mL of the obtained solution was added dropwise to 100 mL of  $\text{Na}_2\text{HPO}_4 \cdot 2\text{H}_2\text{O}$  solution as previously described. Finally, BM10 was obtained after mixing  $\text{NaH}_2\text{PO}_4 \cdot 2\text{H}_2\text{O}$  and  $\text{Mg}(\text{NO}_3)_2 \cdot 6\text{H}_2\text{O}$ , at Mg/P molar ratio 1:1, with the use of the same procedure. Figure 1 presents the experimental procedure.

## 2.3. Characterization Techniques

The mineralogical analysis of the products was carried out qualitatively using an XRD diffractometer-6000 (Shimadzu, Kyoto, Japan) with a cobalt tube and a scanning range 10° to 60° 2-theta at a scan rate of 2°/min. Rietveld refinement [37] of the produced powders was carried out using the software MATCH! (v. 3.11, Crystal Impact, Bonn, Germany). A scanning electron microscope (Inspect F50, FEI Company, Eindhoven, The Netherlands) was used to identify the products morphology. The microscope was equipped with field emission gun electron (FEG) with 1.2 nm resolution and energy dispersive X-ray spectrometer (EDS) with resolution at MnK of 133 eV, to determine the elemental composition of the specimens' surface. The surface chemistry and the elemental analysis of the obtained products were determined by means of X-ray photoelectron spectroscopy using an XPS system (Thermo K Alpha spectrometer, ThermoFisher Scientific, Waltham, MA, USA). The mass loss of each product (~100 mg) during heating between 40 °C and 600 °C, using a heating rate of 5 °C·min<sup>-1</sup> under a helium atmosphere, was determined using a thermogravimetric (TG) analyzer (Netzsch, Selb, Germany, TG 209 F1 Libra).

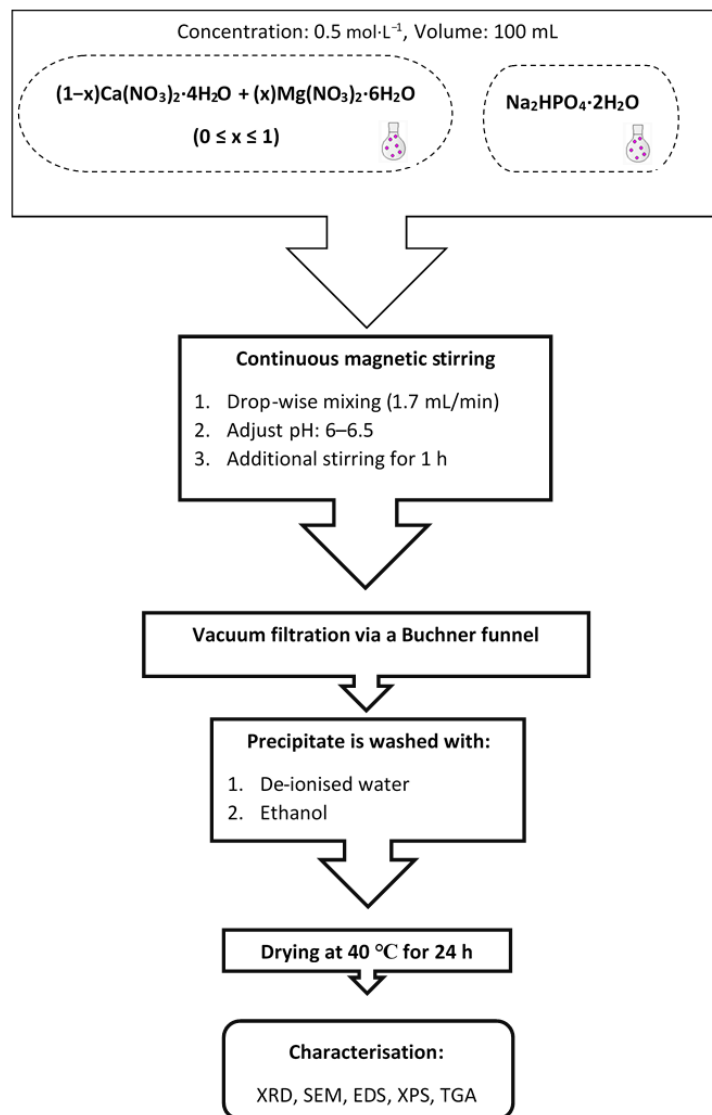


**Figure 1.** Experimental procedure.

### 3. Results and Discussion

#### 3.1. Mineralogical and Microstructural Analysis

The XRD patterns of all produced materials, as well as the patterns of standard brushite and struvite, are shown in Figure 2. The mineralogy of BM0 confirms that this precipitate produced after mixing  $\text{NaH}_2\text{PO}_4 \cdot 2\text{H}_2\text{O}$  and  $\text{Ca}(\text{NO}_3)_2 \cdot 4\text{H}_2\text{O}$  solutions with a Ca:P molar ratio 1:1 (Table 1) is pure brushite, while its crystals grow after nucleation in proportion to the three major planes, namely (020), (121) and (141). All peaks of the BM0 pattern denote the brushite's monoclinic structure [13,38], while the peak at  $11.7^\circ$  2-Theta indicates that the crystal growth takes place primarily along the (020) crystallographic plane [27].

The pattern of BM2 corresponding to the material produced for low Mg/Ca molar ratio (0.25) is similar to the pattern of BM0 and indicates the presence of brushite in which partial replacement of Ca with Mg (Mg doping) takes place. Even though the main brushite peaks are present, their intensity, especially for those associated with the planes (020), (121), and (141), has been affected.

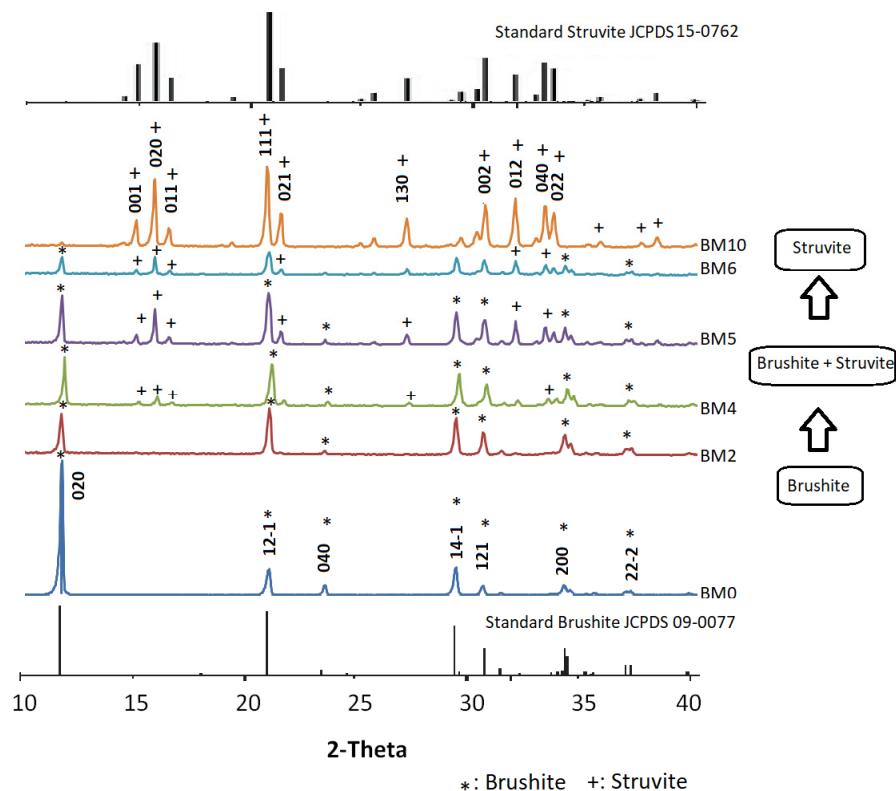
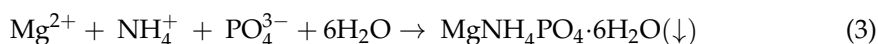
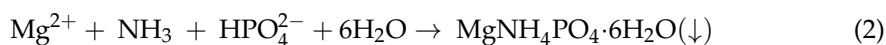


**Figure 2.** XRD patterns of the  $\text{Ca}_{1-x}\text{Mg}_x\cdot\text{HPO}_4\cdot n\text{H}_2\text{O}$  compounds (synthesis details are shown in Table 1).

When the Mg/Ca molar ratio in the starting solution increased gradually from 0.25 to 1.0 and eventually to 1.5 (patterns BM4 to BM6) the degree of Ca replacement with Mg increased while in parallel struvite started to precipitate. Thus, the respective XRD patterns show that at higher Mg/Ca molar ratios the intensity of struvite peaks increases. Finally, the pattern of BM10 of the precipitate formed when a Mg/P ratio of 1.0 was used confirms the presence of pure struvite,  $\text{NH}_4\text{MgPO}_4\cdot 6\text{H}_2\text{O}$ , with orthorhombic crystal structure as compared with the standard struvite pattern (JCPDS file No.15–0762) [39,40]. The XRD results of the present study match almost perfectly the XRD patterns of Mg doped brushite, for doping percentages varying between 5% and 50%, as shown in a very recent study [26].

Struvite is formed through the following equations:



It is known that the consumption of  $\text{NH}_3$  and thus the formation (precipitation) of struvite lowers the solution pH and thus equilibrium is shifted towards increased concentrations of  $\text{NH}_4^+$  ions. Also, the presence of other ions as well as changes in temperature, which is not the case in the present study, can affect the ion speciation characteristics [41,42].

Rietveld refined unit cell parameters for brushite- and struvite-rich materials are presented in Tables 2 and 3. It is seen that for the materials BM0–BM5 (Table 2), produced with the use of Mg/Ca molar ratio in the starting solution up to 1.0 and in which brushite was the dominant phase formed, unit cell parameters are almost constant and exhibited a slight increasing trend. On the other hand, for the materials BM6 and BM10, in which struvite was the dominant phase, unit cell parameters exhibited were also constant and exhibited a slight decreasing trend. The relatively minor cell shrinkage noticed may be explained by the fact that  $\text{Mg}^{2+}$  ions have a smaller ionic radius compared to  $\text{Ca}^{2+}$  ions.

The quality of the Rietveld refinement was acceptable for all materials studied ( $R_{\text{Brag}} < 8\%$ ,  $\chi^2 < 2$ ). These data are similar to the data obtained in earlier recent studies focusing on the production of brushite or struvite [26,43,44].

**Table 2.** Refined unit cell parameters for brushite from XRD data using the Rietveld approach \*.

Product ID	Brushite wt%	<i>a</i> (Å)	<i>b</i> (Å)	<i>c</i> (Å)	( $\beta^\circ$ )	<i>V</i> (Å <sup>3</sup> )
BM0	100.0	5.8145	15.1693	6.2399	116.392	492.83
BM2	100.0	5.8165	15.1904	6.2465	116.382	492.78
BM4	100.0	5.8191	15.1908	6.2518	116.403	492.51
BM5	97.1	5.8160	15.1764	6.2482	116.429	492.01
BM6	20.9	5.8153	15.1677	6.2470	116.442	
BM10	0.0	-	-	-	-	

*a*, *b*, *c*,  $\beta^\circ$ : unit cell parameters (monoclinic crystal system), *V*: unit cell volume, \* Standard deviation varied between 0.001 and 0.005 for all samples.

**Table 3.** Refined unit cell parameters for struvite from XRD data using the Rietveld approach \*.

Product ID	Struvite wt%	<i>a</i> (Å)	<i>b</i> (Å)	<i>c</i> (Å)	<i>V</i> (Å <sup>3</sup> )
BM0	0.0	-	-	-	-
BM2	0.0	-	-	-	-
BM4	0.0	-	-	-	-
BM5	2.9	6.9560	6.1378	11.2041	-
BM6	79.1	6.9589	6.1364	11.2034	478.12
BM10	100.0	6.9501	6.1359	11.2014	477.54

*a*, *b*, *c*: unit cell parameters (orthorhombic crystal system), *V*: unit cell volume, \* Standard deviation varied between 0.001 and 0.005 for all samples.

In Figure 3, SEM images of the various  $\text{Ca}_{1-x}\text{Mg}_x\text{HPO}_4 \cdot n\text{H}_2\text{O}$  compounds, obtained for different Mg/Ca molar ratios present in solution, are shown. Figure 3a–c shows the morphology of pure brushite (BM0), as well as of biphasic compounds (BM5) and pure struvite (BM10). More specifically, Figure 3a (BM0 with Ca/P molar ratio 1.0) indicates the precipitation of plate-like brushite crystals. It is known that the morphology of brushite is characterized by a plate-like or needle like structure, depending on the solution pH used [11,12]. The plate-like crystals are thin (~400 nm), while their width and elongation are approximately 10  $\mu\text{m}$  and 20  $\mu\text{m}$ , respectively, values similar to those reported in other studies [45–47]. When the Mg/Ca molar ratio increases and thus a higher degree of Ca replacement with Mg as well as struvite precipitation (BM5) takes place, brushite crystals with smaller length, ranging between ~2  $\mu\text{m}$  and ~10  $\mu\text{m}$  in the direction (020) are formed (Figure 3b), as is also indicated in earlier studies [11]. Finally, Figure 3c shows that BM10 is composed of orthorhombic struvite crystals with a length of ~20  $\mu\text{m}$  [40,48]. It is underlined that the SEM analysis confirms the XRD results as shown in Figure 2.

As shown in Figure 4a, in the brushite crystals (BM0) the weight percentages of O, Ca and P were 67.42, 17.83 and 14.74 wt% which are close to the theoretical ones, namely 55.80, 23.25 and 18.20 wt% respectively. These weight percentages denote a Ca/P molar ratio of 1.0, equal to the theoretical ratio in brushite and the one present in the starting solution (Table 1). Figure 4b shows that in the brushite plate-like crystals in BM5, which were formed using a Mg/P molar ratio of 0.5 in the starting solution, the weight percentages of O, Ca and P were 62.44, 18.04 and 16.21 wt% respectively, while those of Mg and Na were 2.39 and 0.91 wt% respectively. These percentages prove that the plate-like brushite crystals have a smaller Mg/P molar ratio, 0.20, indicating that only a percentage of the Mg present in the solution replaced Ca in brushite, while the rest was precipitated as struvite as also shown in the respective XRD pattern in Figure 2 and reported in earlier studies [49–51]. As a result of Mg doping, the Ca/P molar ratio in BM5 decreased from 1.0 in BM0 to 0.86. It is also mentioned that the presence of Na in BM5 is probably due to the precipitation

of  $\text{Na}_2(\text{CO}_3)_2$  or due to partial incorporation of Na. The role of Na incorporation into the lattice of the produced materials is very important since it increases their thermal stability and enables their use as bioceramics in medical applications [24,52]. However, the elucidation of Na incorporation and its effect on the properties of the (bio)materials needs to be further investigated. Finally, as shown in Figure 4c, the weight percentages of P and Mg in BM10 were 18.51 and 11.34 wt% respectively, indicating a Mg/P molar ratio in the produced material of 0.83 which is close to the theoretical value of 1.0 present in pure struvite. The results of EDS analysis for brushite- and struvite-rich phases, in term of the main molar ratios, are quite similar to those indicated in earlier recent studies [53–57].

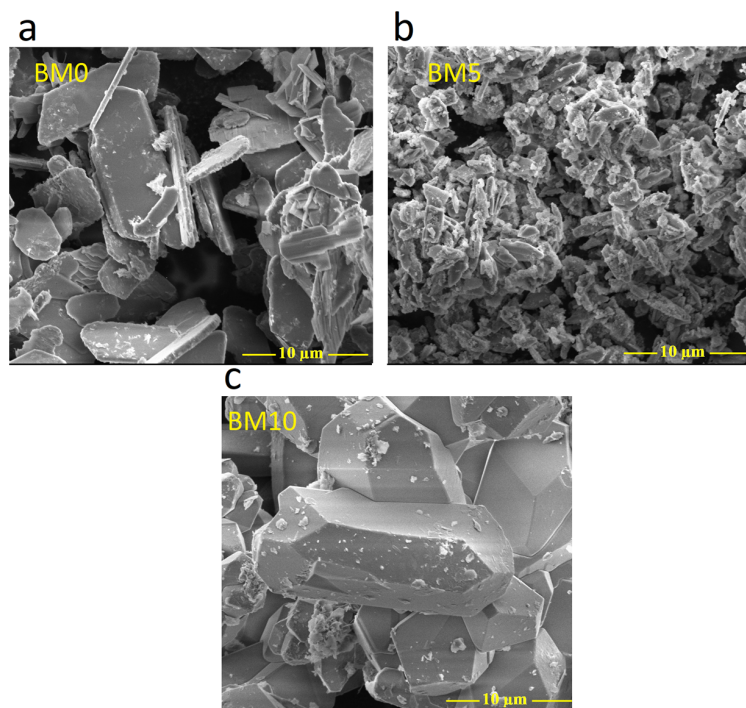


Figure 3. SEM images of  $\text{Ca}_{1-x}\text{Mg}_x\text{HPO}_4 \cdot n\text{H}_2\text{O}$  compounds, (a) BM0, (b) BM5, and (c) BM10.

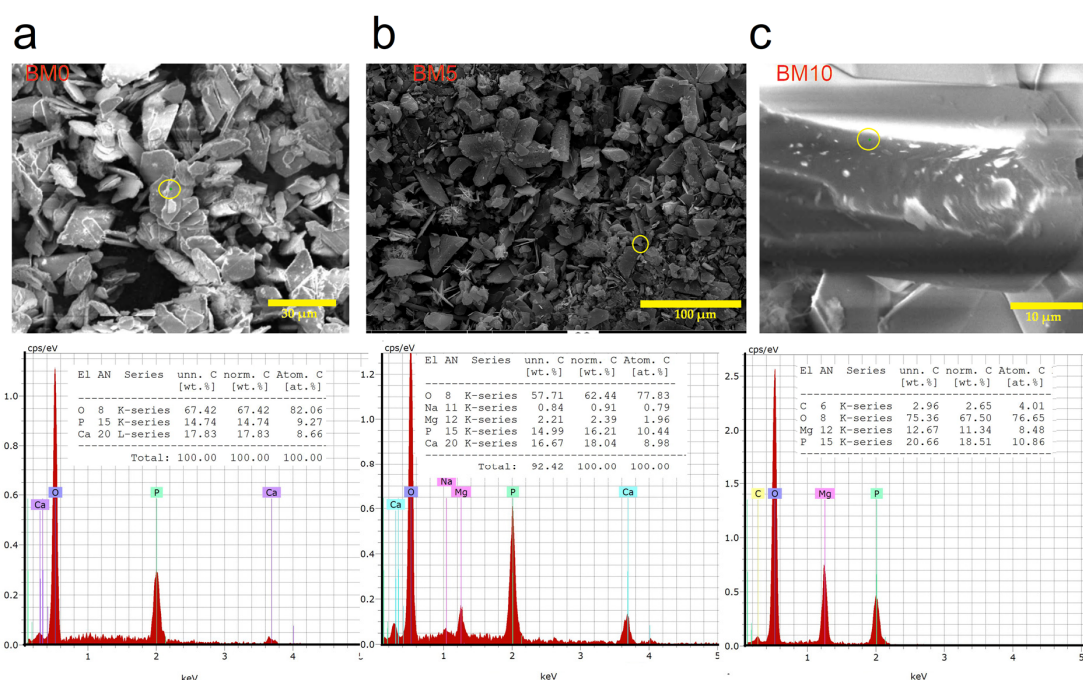
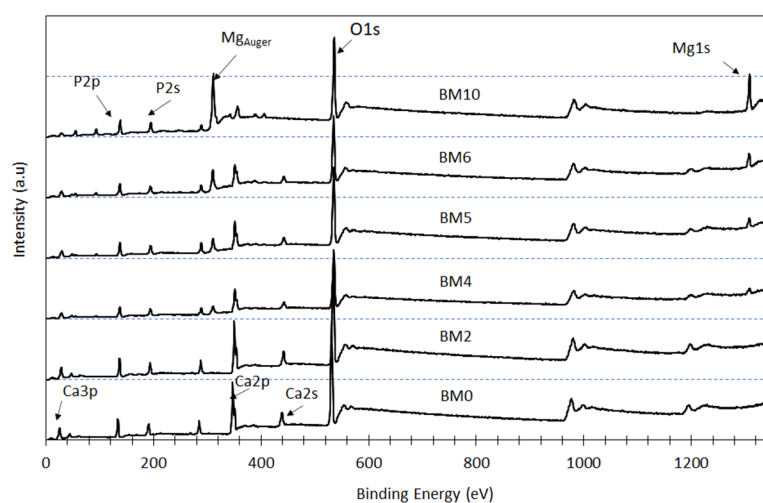


Figure 4. EDS analysis of (a) BM0, (b) BM5 and (c) BM10 compounds.

### 3.2. Elemental and Chemical Composition of $\text{Ca}_{1-x}\text{Mg}_x\cdot\text{HPO}_4\cdot n\text{H}_2\text{O}$ Compounds

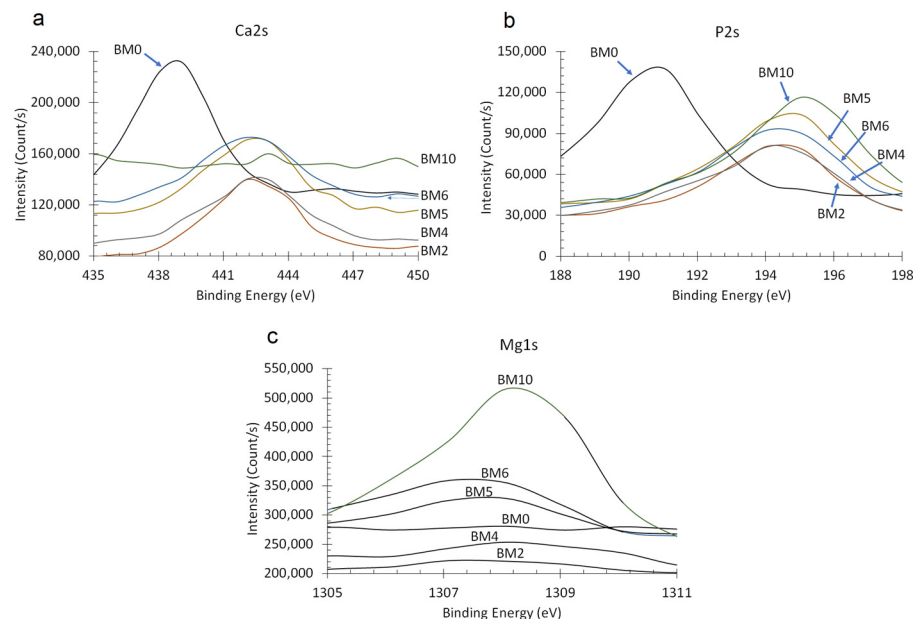
XPS analysis was carried out to evaluate the effect of the Mg/Ca ratio present in the starting solution on the surface chemistry and chemical state of the elements P, Ca, and Mg in the synthesized  $\text{Ca}_{1-x}\text{Mg}_x\text{HPO}_4\cdot n\text{H}_2\text{O}$  compounds (Figure 5); as mentioned earlier this ratio affects the degree of replacement of Ca with Mg in brushite as well as the precipitation of pure struvite (when higher ratios are used). Peaks of Mg1s and Mg auger are clearly shown in the XPS spectra of the products obtained when higher Mg/Ca molar ratios are used. Thus, as shown in the BM4 to BM10 spectra, when this ratio increases gradually the intensity of the Mg1s peaks also increases, while the intensity of Ca2s and Ca2p peaks decreases almost proportionally. On the other hand, almost no change is noticed in the intensity of the P2s peaks. These observations confirm that the intensity of P, Ca, and Mg peaks depends on the degree of Ca replacement with Mg as well as on the amount of the precipitated struvite (for higher Mg/Ca ratios).



**Figure 5.** XPS spectra of  $\text{Ca}_{1-x}\text{Mg}_x\cdot\text{HPO}_4\cdot n\text{H}_2\text{O}$  compounds.

The effect of Mg/Ca ratio on the binding energies of Ca2s, P2s and Mg1s peaks is shown in Figure 6a–c, respectively. Thus, when the Mg/Ca ratio in the starting solution is kept low (0.25) the partial replacement of Ca with Mg (BM2 compound) resulted in a slight increase of the binding energies of P2s and Ca2s peaks, from 190 eV to 194 eV and from 438 eV to 442 eV, respectively. When the Mg/Ca ratio further increased to 0.67 (BM4 compound) and eventually to 1.5 (BM6 compound) a noticeable increase in the intensity of Mg1s is shown. As mentioned earlier, the gradual increase of this ratio results in an increase of the rate of replacement of Ca with Mg as well as in the precipitation of pure struvite. As the XRD pattern confirms (Figure 2), BM4 is the first compound formed that contains struvite-like crystals. BM10 which is pure struvite is characterized by Mg1s and Mg auger peaks of the highest intensity.

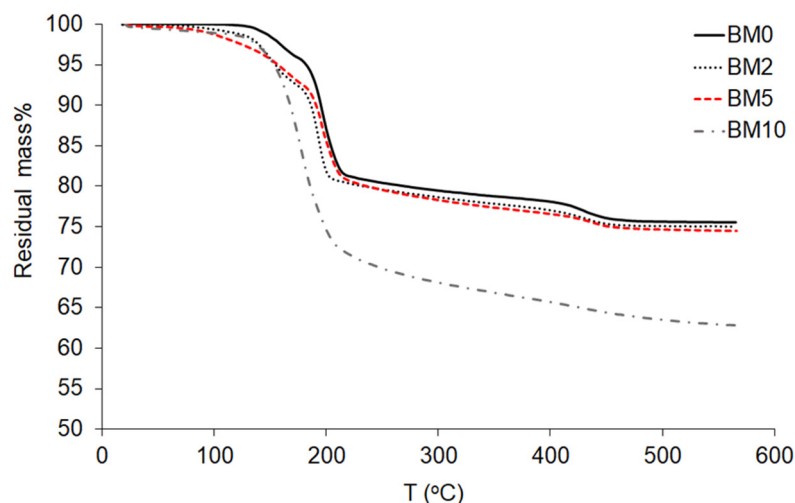
The XPS results confirm that at low Mg/Ca ratios in the starting solution Ca is partially replaced by Mg and alters the crystal structure of the  $\text{Ca}_{1-x}\text{Mg}_x\text{HPO}_4\cdot n\text{H}_2\text{O}$  compounds by increasing the binding energies of Ca2s and P2s peaks [58]. It is obvious that as the Mg concentration in the starting solution increases and the respective one of Ca decreases, supersaturation decreases with respect to brushite and increases with respect to struvite, thus mixed phases precipitate favoring eventually the formation of pure struvite when no Ca is present in the system (BM10 compound).



**Figure 6.** XPS analysis of the chemical state of (a) P2s, (b) Ca2s, and (c) Mg1s in  $\text{Ca}_{1-x}\text{Mg}_x\text{HPO}_4 \cdot n\text{H}_2\text{O}$  compounds.

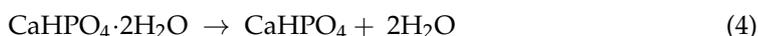
### 3.3. Thermo-Gravimetric Analysis (TGA)

Figure 7 shows the results of the TGA analysis for the compounds BM0 to BM10. Brushite is classified as a water-bearing phosphate [47] and its crystal structure contains compact sheets consisting of parallel chains in which Ca ions are coordinated by six phosphate ions and two oxygen atoms belonging to the water molecules [59]. Brushite contains two water molecules in its lattice and adsorbed water molecules on its surface, as indicated by the presence of two sharp peaks of mass loss during heating between 80–220 °C [60,61]. Part of the chemically-bound water is released during the transformation of brushite to monetite,  $\text{CaHPO}_4$ , at ~220 °C [62], and later to calcium pyrophosphate,  $\text{Ca}_2\text{P}_2\text{O}_7$ , at ~400 °C [8]. Pyrophosphates are decomposed at higher temperatures of 750–800 °C [63]. Heating of pure brushite (BM0) to 600 °C results in a mass loss of approximately 25 wt%, while the theoretical mass loss for the dehydration of brushite is 20.93 wt% [64]. It is thus seen that, when low to average Mg/Ca ratios are present in the starting solution and partial replacement of Ca with Mg takes place, while the formation of struvite is limited (BM2–BM5 compounds), the mass loss during heating is very similar to the value determined for brushite.



**Figure 7.** TG curves of  $\text{Ca}_{1-x}\text{Mg}_x\text{HPO}_4 \cdot n\text{H}_2\text{O}$  compounds (BM0–BM10).

Dehydration of brushite over the temperature range 110–215 °C takes place according to Equation (4) and normally results in a weight loss of about 19 wt%, while the formation of calcium pyrophosphate is accomplished by Equation (5).



The mass loss determined for pure struvite (BM10) is higher and reaches 38 wt%, which is lower than the theoretical value of ~52% for the complete de-volatilization of struvite and the formation of Mg-pyrophosphate ( $\text{Mg}_2\text{P}_2\text{O}_7$ ) [65–67]. The mass loss of struvite is due to the loss of moisture, the release of crystallization water and ammonia and the percentage recorded in this study is similar to the percentage indicated in an earlier study for the decomposition of dittmarite,  $\text{Mg}(\text{NH}_4)(\text{PO}_4) \cdot \text{H}_2\text{O}$  [41]. The decomposition of struvite takes place according to the following Equation (6):

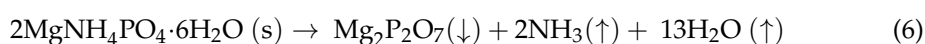
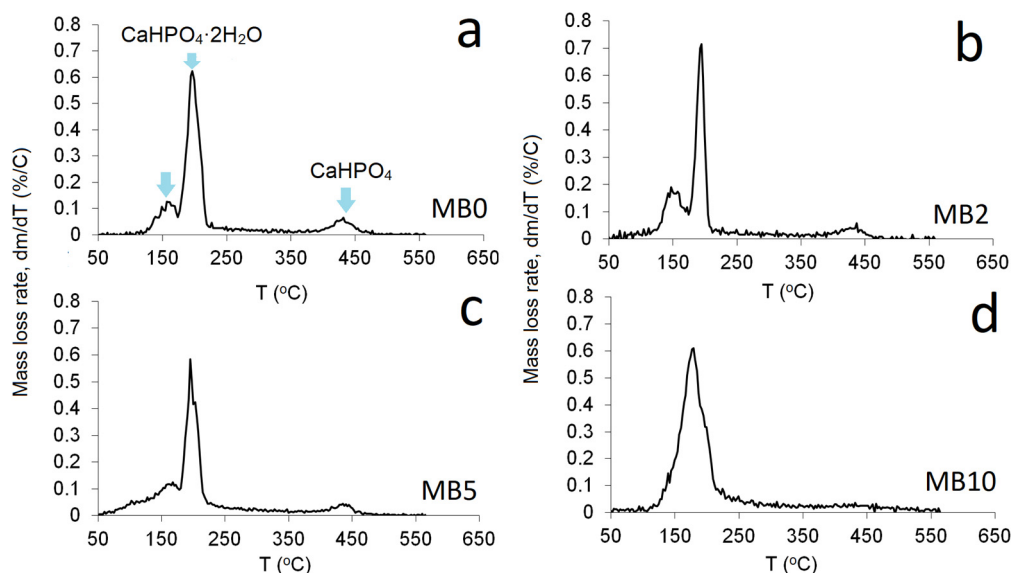


Figure 8 shows the rate of mass loss as a function of heating temperature for  $\text{Ca}_{1-x}\text{Mg}_x\text{HPO}_4 \cdot n\text{H}_2\text{O}$  compounds. More specifically, Figure 8a–c shows the dehydration peaks corresponding to the two water molecules of pure brushite (BM0), as well as of the compounds produced with the use of Mg/Ca ratios 0.25 and 1.0 (BM2 and BM5 respectively), which are characterized by partial replacement of Ca with Mg as well as the limited production of struvite. It is seen that when the Mg/Ca ratio in the starting solution increases to 1.0 (BM5, Figure 8c), one primary zone of mass loss at approximately 180 °C is shown. On the other hand, Figure 8d shows the loss of structural water of struvite (BM10) for which the overall mass loss at 500 °C was approximately 38%.



**Figure 8.** Differential Thermogravimetric Analysis (TGA) of  $\text{Ca}_{1-x}\text{Mg}_x\text{HPO}_4 \cdot n\text{H}_2\text{O}$  compounds (a) BM0, (b) BM2, (c) BM5, (d) BM10.

### 3.4. Phase Evolution during the Precipitation of $\text{Ca}_{1-x}\text{Mg}_x\text{HPO}_4 \cdot n\text{H}_2\text{O}$ Compounds

The results of this study demonstrated that when the Mg/Ca ratio in the starting solution is up to 0.25, Mg replaces Ca in the brushite lattice (MB2) and the original shape of plate-like brushite crystals (BM0) is preserved [68,69]. Besides, no struvite is formed as deduced by the use of analytical techniques. The main difference noticed is the decrease of the brushite crystal size, because magnesium, despite the fact that it does not

seem to noticeably affect process kinetics, inhibits crystal growth, as mentioned in earlier studies [70,71].

When the Mg/Ca ratio increases to 0.67 and eventually to 1.0 (BM4–MB5) apart from Mg-doped brushite, struvite,  $\text{NH}_4\text{MgPO}_4 \cdot 6\text{H}_2\text{O}$ , with orthorhombic crystals starts to precipitate [41,51,72]. At higher Mg/Ca ratios (1.5) due to the decrease of saturation with respect to brushite and the increase of saturation with respect to struvite, brushite crystals gradually disappear and struvite crystals with size of approximately 20  $\mu\text{m}$  appear (BM6). When no Ca is present in the starting solution, pure struvite precipitates (BM10). These data are summarized in the following Table 4.

**Table 4.** Phase evolution, crystal size and structure as function of Mg/Ca molar ratio in solution.

Mg/Ca Ratio	Crystal Structure	Crystal Size ( $\mu\text{m}$ )	Compounds Formed
$\leq 0.25$	Plate-like	~10	Brushite
$0.25 < x \leq 1.5$	Plate-like orthorhombic	~2	Brushite + Struvite
$> 1.5$	Orthorhombic	~20	Struvite

#### 4. Conclusions

In this study, the evolution of the degree of replacement of Ca with Mg in brushite, for the production of  $\text{Ca}_{1-x}\text{Mg}_x\text{HPO}_4 \cdot n\text{H}_2\text{O}$  materials was investigated and elucidated with the use of XRD, TG, SEM-EDS and XPS analysis.

It has been shown that when the Mg/Ca molar ratio is low (up to 0.40) in the starting solution, partial replacement of Ca with Mg takes place which does not practically affect the structure of the precipitated brushite. When the Mg/Ca molar ratio gradually increases to 1.5 and the solution superstition with respect to Mg increases, in addition to Mg-doped brushite, orthorhombic struvite,  $\text{NH}_4\text{MgPO}_4 \cdot 6\text{H}_2\text{O}$ , precipitates.

The results of this study provide useful insights for the future synthesis of biomaterials with specific composition and tailored properties, by controlling the Mg/Ca ratio in the starting solution. However, additional studies need to be carried out in order to elucidate several aspects related to the performance of the produced biomaterials. Factors including biological and mechanical performance as well as physicochemical and antibacterial properties need to be carefully investigated. Also, the effect of doping with additional ions needs to be in depth investigated since specific ions may exhibit either beneficial or detrimental effects on the final properties of the produced biomaterials.

**Author Contributions:** Conceptualization, M.A.; methodology, M.A. and S.A.M.; validation, K.K., M.A. and A.A.; formal analysis, K.K.; powder synthesis and characterization, A.A., A.S.A. and S.A.M.; investigation, M.A. and K.K.; resources, A.S.A., K.I. and M.E.M.; data curation, S.A.M. and A.A.; writing—original draft preparation, M.A.; writing—review and editing, K.K.; supervision, K.K., M.A. and K.I. All authors have read and agreed to the published version of the manuscript.

**Funding:** This research received no external funding.

**Institutional Review Board Statement:** Not applicable.

**Informed Consent Statement:** Not applicable.

**Data Availability Statement:** The data presented in this study are available on request from the corresponding author. Most of this data is obtained after the use of analytical techniques (XRD, TG, SEM-EDS, XRS).

**Acknowledgments:** The authors would like to acknowledge the efforts and contribution of four anonymous reviewers in clarifying several aspects and improving the quality of the paper.

**Conflicts of Interest:** The authors declare no conflict of interest.

## References

1. Alshaaer, M.; Kailani, M.H.; Ababneh, N.; Abu Mallouh, S.A.; Sweileh, B.; Awidi, A. Fabrication of porous bioceramics for bone tissue applications using luffa cylindrical fibres (LCF) as template. *Process. Appl. Ceram.* **2017**, *11*, 13–20. [[CrossRef](#)]
2. Radwan, N.H.; Nasr, M.; Ishak, R.A.; Abdeltawa, N.F.; Awad, G.A. Chitosan-calcium phosphate composite scaffolds for control of postoperative osteomyelitis: Fabrication, characterization, and in vitro–in vivo evaluation. *Carbohydr. Polym.* **2020**, *244*, 116482. [[CrossRef](#)] [[PubMed](#)]
3. Alshaaer, M.; Kailani, M.H.; Jafar, H.; Ababneh, N.; Awidi, A. Physicochemical and Microstructural Characterization of Injectable Load-Bearing Calcium Phosphate Scaffold. *Adv. Mater. Sci. Eng.* **2013**, 149261. [[CrossRef](#)]
4. Hurle, K.; Oliveira, J.; Reis, R.; Pina, S.; Goetz-Neunhoeffler, F. Ion-doped Brushite Cements for Bone Regeneration. *Acta Biomater.* **2021**. [[CrossRef](#)]
5. Khalifehzadeh, R.; Arami, H. Biodegradable calcium phosphate nanoparticles for cancer therapy. *Adv. Colloid Interface Sci.* **2020**, *279*, 102157. [[CrossRef](#)]
6. Shyong, Y.; Chang, K.; Lin, F. Calcium phosphate particles stimulate exosome secretion from phagocytes for the enhancement of drug delivery. *Colloid Surf. B* **2018**, *1711*, 391–397. [[CrossRef](#)]
7. Liu, Y.; Ma, R.; Li, D.; Qi, C.; Han, L.; Chen, M.; Fu, F.; Yuan, J.; Li, G. Effects of calcium magnesium phosphate fertilizer, biochar and spent mushroom substrate on compost maturity and gaseous emissions during pig manure composting. *J. Environ. Manag.* **2020**, *267*, 110649. [[CrossRef](#)]
8. Alshaaer, M.; Cuyppers, H.; Mosselmans, G.; Rahier, H.; Wastiels, J. Evaluation of a low temperature hardening Inorganic Phosphate Cement for high-temperature applications. *Cement Concrete Res.* **2011**, *41*, 38–45. [[CrossRef](#)]
9. Moukannaa, S.; Nazari, A.; Bagheri, A.; Loutou, M.; Sanjayan, J.G.; Hakkou, R. Alkaline fused phosphate mine tailings for geopolymer mortar synthesis: Thermal stability, mechanical and microstructural properties. *J. Non Cryst. Solids* **2019**, *511*, 76–85. [[CrossRef](#)]
10. Kinnunen, P.; Ismailov, A.; Solismaa, S.; Sreenivasan, H.; Räisänen, M.-L.; Levänen, E.; Illikainen, M. Recycling mine tailings in chemically bonded ceramics—A review. *J. Clean. Prod.* **2018**, *174*, 634–649. [[CrossRef](#)]
11. Alkhraisat, M.H.; Rueda, C.; Cabarcos, E.L. Strontium Ions Substitution in Brushite Crystals: The Role of Strontium Chloride. *J. Funct. Biomater.* **2011**, *2*, 31–38. [[CrossRef](#)] [[PubMed](#)]
12. Xue, Z.; Wang, Z.; Sun, A.; Huang, J.; Wu, W.; Chen, M.; Hao, X.; Huang, Z.; Lin, X.; Weng, S. Rapid construction of polyetheretherketone (PEEK) biological implants incorporated with brushite (CaHPO<sub>4</sub>·2H<sub>2</sub>O) and antibiotics for anti-infection and enhanced osseointegration. *Mater. Sci. Eng. C Mater.* **2020**, *111*. [[CrossRef](#)]
13. Kim, Y.; Lee, S.Y.; Roh, Y.; Lee, J.; Kim, J.; Lee, Y.; Bang, J.; Lee, Y.J. Optimizing Calcium Phosphates by the Control of pH and Temperature via Wet Precipitation. *J. Nanosci. Nanotechnol.* **2015**, *15*, 10008–10016. [[CrossRef](#)] [[PubMed](#)]
14. Luo, J.; Engqvist, H.; Persson, C. A ready-to-use acidic, brushite-forming calcium phosphate cement. *Acta Biomater.* **2018**, *81*, 304–314. [[CrossRef](#)]
15. Mert, I.; Mandel, S.; Tas, A.C. Do cell culture solutions transform brushite (CaHPO<sub>4</sub>·2H<sub>2</sub>O) to octacalcium phosphate (Ca<sub>8</sub>(HPO<sub>4</sub>)<sub>2</sub>(PO<sub>4</sub>)<sub>4</sub>·5H<sub>2</sub>O). In *Advances in Bioceramics and Porous Ceramics IV*; Narayan, R., Colombo, P., Eds.; John Wiley & Sons Inc.: Hoboken, NJ, USA, 2011; pp. 79–94. [[CrossRef](#)]
16. Patil, S.B.; Jena, A.; Bhargava, P. Influence of Ethanol Amount during Washing on Deagglomeration of Co-Precipitated Calcined Nanocrystalline 3YSZ Powders. *Int. J. Appl. Ceram. Technol.* **2013**, *10*, E247–E257. [[CrossRef](#)]
17. Piva, R.H.; Piva, D.H.; Pierri, J.; Montedo, O.R.K.; Morelli, M.R. Azeotropic distillation, ethanol washing, and freeze drying on coprecipitated gels for production of high surface area 3Y-TZP and 8YSZ powders: A comparative study. *Ceram. Int.* **2015**, *41*, 14148–14156. [[CrossRef](#)]
18. Mirtchi, A.A.; Lemaitre, J.; Terao, N. Calcium phosphate cements: Study of the β-tricalcium phosphate—monocalcium phosphate system. *Biomaterials* **1989**, *10*, 475–480. [[CrossRef](#)]
19. Pina, S.; Olhero, S.; Gheduzzi, S.; Miles, A.; Ferreira, J. Influence of setting liquid composition and liquid-to-powder ratio on properties of a Mg-substituted calcium phosphate cement. *Acta Biomater.* **2009**, *5*, 1233–1240. [[CrossRef](#)] [[PubMed](#)]
20. Lagier, R.; Baud, C.A. Magnesium Whitlockite, a Calcium Phosphate Crystal of Special Interest in Pathology. *Pathol. Res. Pract.* **2003**, *199*, 329–335. [[CrossRef](#)] [[PubMed](#)]
21. Kannan, S.; Goetz-Neunhoeffler, F.; Neubauer, J.; Ferreira, J.M.F. Ionic Substitutions in Biphasic Hydroxyapatite and β-Tricalcium Phosphate Mixtures: Structural Analysis by Rietveld Refinement. *J. Am. Ceram. Soc.* **2008**, *91*, 1–12. [[CrossRef](#)]
22. Kannan, S.; Goetz-Neunhoeffler, F.; Neubauer, J.; Rebelo, A.H.S.; Valério, P.; Ferreira, J.M.F. Rietveld structure and in vitro analysis on the influence of magnesium in biphasic (hydroxyapatite and β-tricalcium phosphate) mixtures. *J. Biomed. Mater. Res. Part B Appl. Biomater.* **2009**, *90*, 404–411. [[CrossRef](#)]
23. Kannan, S.; Lemos, A.F.; Rocha, J.H.G.; Ferreira, J.M.F. Characterization and Mechanical Performance of the Mg-Stabilized β-Ca<sub>3</sub>(PO<sub>4</sub>)<sub>2</sub> Prepared from Mg-Substituted Ca-Deficient Apatite. *J. Am. Ceram. Soc.* **2006**, *89*, 2757–2761. [[CrossRef](#)]
24. Kannan, S.; Ferreira, J.M.F. Synthesis and Thermal Stability of Hydroxyapatite–β-Tricalcium Phosphate Composites with Cosubstituted Sodium, Magnesium, and Fluorine. *Chem. Mater.* **2006**, *18*, 198–203. [[CrossRef](#)]
25. Torres, P.M.C.; Abrantes, J.C.C.; Kaushal, A.; Pina, S.; Döbelin, N.; Bohner, M.; Ferreira, J.M.F. Influence of Mg-doping, calcium pyrophosphate impurities and cooling rate on the allotropic α ↔ β—tricalcium phosphate phase transformations. *J. Eur. Ceram. Soc.* **2016**, *36*, 817–827. [[CrossRef](#)]

26. Sayahi, M.; Santos, J.; El-Feki, H.; Charvillat, C.; Bosc, F.; Karacan, I.; Milthorpe, B.; Drouet, C. Brushite (Ca,M)HPO<sub>4</sub>·2H<sub>2</sub>O doping with bioactive ions (M = Mg<sup>2+</sup>, Sr<sup>2+</sup>, Zn<sup>2+</sup>, Cu<sup>2+</sup>, and Ag<sup>+</sup>): A new path to functional biomaterials? *Mater. Today Chem.* **2020**, *16*, 100230. [[CrossRef](#)]
27. Wu, F.; Wei, J.; Guo, H.; Chen, F.; Hong, H.; Liu, C. Self-setting bioactive calcium-magnesium phosphate cement with high strength and degradability for bone regeneration. *Acta Biomater.* **2008**, *4*, 1873–1884. [[CrossRef](#)]
28. Qi, T.; Weng, J.; Yu, F.; Zhang, W.; Li, G.; Qin, H.; Tan, Z.; Zeng, H. Insights into the Role of Magnesium Ions in Affecting Osteogenic Differentiation of Mesenchymal Stem Cells. *Biol. Trace Elem. Res.* **2021**, *199*, 559–567. [[CrossRef](#)]
29. Ding, S.; Zhang, J.; Tian, Y.; Huang, B.; Yuan, Y.; Liu, C. Magnesium modification up-regulates the bioactivity of bone morphogenetic protein-2 upon calcium phosphate cement via enhanced BMP receptor recognition and Smad signaling pathway. *Colloids Surf. B Biointerfaces* **2016**, *145*, 140–151. [[CrossRef](#)]
30. Kazimierzczak, P.; Kolmas, J.; Przekora, A. Biological Response to Macroporous Chitosan-Agarose Bone Scaffolds Comprising Mg- and Zn-Doped Nano-Hydroxyapatite. *Int. J. Mol. Sci.* **2019**, *20*, 3835. [[CrossRef](#)]
31. Kannan, S.; Goetz-Neunhoeffer, F.; Neubauer, J.; Pina, S.; Torres, P.M.C.; Ferreira, J.M.F. Synthesis and structural characterization of strontium—and magnesium-co-substituted b-tricalcium phosphate. *Acta Biomater.* **2010**, *6*, 571–576. [[CrossRef](#)]
32. Smoak, M.M.; Mikos, A.G. Advances in biomaterials for skeletal muscle engineering and obstacles still to overcome. *Mater. Today Bio* **2020**, *7*, 100069. [[CrossRef](#)] [[PubMed](#)]
33. Afewerki, S.; Bassous, N.; Harb, S.; Palo-Nieto, C.; Ruiz-Esparza, G.U.; Marciano, F.R.; Webster, T.J.; Furtado, A.S.A.; Lobo, A.O. Advances in dual functional antimicrobial and osteoinductive biomaterials for orthopaedic applications. *Nanomedicine* **2020**, *24*, 102143. [[CrossRef](#)]
34. Liu, T.; Xu, J.; Pan, X.; Ding, Z.; Xie, H.; Wang, X.; Xie, H. Advances of adipose-derived mesenchymal stem cells-based biomaterial scaffolds for oral and maxillofacial tissue engineering. *Bioact. Mater.* **2021**, *6*, 2467–2478. [[CrossRef](#)]
35. Liang, Y.; Luan, X.; Liu, X. Recent advances in periodontal regeneration: A biomaterial perspective. *Bioact. Mater.* **2020**, *5*, 297–308. [[CrossRef](#)] [[PubMed](#)]
36. Lu, B.-Q.; Willhammar, T.; Sun, B.; Hedin, N.; Gale, J.D.; Gebauer, D. Introducing the crystalline phase of dicalcium phosphate monohydrate. *Nat. Commun.* **2020**, *11*, 1546. [[CrossRef](#)] [[PubMed](#)]
37. Cheary, R.W.; Coelho, A.A. A Fundamental Parameters Approach of X-Ray Line-Profile Fitting. *J. Appl. Cryst.* **1992**, *25*, 109–121. [[CrossRef](#)]
38. Nosrati, H.; Le, D.Q.S.; Enameh, R.Z.; Perez, M.C.; Bünger, C.E. Nucleation and growth of brushite crystals on the graphene sheets applicable in bone cement. *Bol. Soc. Esp. Cerám. Vidr.* **2020**. [[CrossRef](#)]
39. Li, H.; Yao, Q.-Z.; Wang, Y.-Y.; Li, Y.-L.; Zhou, G.-T. Biomimetic synthesis of struvite with biogenic morphology and implication for pathological biomineralization. *Sci. Rep.* **2015**, *5*, 7718. [[CrossRef](#)] [[PubMed](#)]
40. Yang, H.; Martinelli, L.; Tasso, F.; Sprocati, A.R.; Pinzari, F.; Liu, Z.; Downs, R.T.; Sun, H.J. A new biogenic, struvite-related phosphate, the ammonium-analog of hazenite, (NH<sub>4</sub>)NaMg<sub>2</sub>(PO<sub>4</sub>)<sub>2</sub>·14H<sub>2</sub>O. *Am. Mineral.* **2014**, *99*, 1761–1766. [[CrossRef](#)]
41. Tansel, T.; Lunn, G.; Monje, O. Struvite formation and decomposition characteristics for ammonia and phosphorus recovery: A review of magnesium-ammonia-phosphate interactions. *Chemosphere* **2018**, *194*, 504–514. [[CrossRef](#)]
42. Schuiling, R.D.; Andrade, A. Recovery of struvite from calf manure. *Environ. Technol.* **1999**, *20*, 765–768. [[CrossRef](#)]
43. Meira, R.C.S.; Paz, S.P.A.; Corrêa, J.A.M. XRD-Rietveld analysis as a tool for monitoring struvite analog precipitation from wastewater: P, Mg, N and K recovery for fertilizer production. *J. Mater. Res. Technol.* **2020**, *9*, 15202–15213. [[CrossRef](#)]
44. Yan, H.; Shih, K. Effects of calcium and ferric ions on struvite precipitation: A new assessment based on quantitative X-ray diffraction analysis. *Water Res.* **2016**, *95*, 310–318. [[CrossRef](#)] [[PubMed](#)]
45. Alshaaer, M. Microstructural characteristics and long-term stability of wollastonite-based chemically bonded phosphate ceramics. *Int. J. Appl. Ceram. Technol.* **2021**, *18*, 319–331. [[CrossRef](#)]
46. Kumar, M.; Xie, J.; Chittur, K.; Riley, C. Transformation of modified brushite to hydroxyapatite in aqueous solution: Effects of potassium substitution. *Biomaterials* **1999**, *20*, 1389–1399. [[CrossRef](#)]
47. Tamimi, F.; Le Nihouannen, D.; Eimar, H.; Sheikh, Z.; Komarova, S.; Barralet, J. The effect of autoclaving on the physical and biological properties of dicalcium phosphate dihydrate bioceramics: Brushite vs. monetite. *Acta Biomater.* **2012**, *8*, 3161–3169. [[CrossRef](#)] [[PubMed](#)]
48. Thant Zin, M.M.; Kim, D.-J. Simultaneous recovery of phosphorus and nitrogen from sewage sludge ash and food wastewater as struvite by Mg-biochar. *J. Hazard. Mater.* **2021**, *403*, 123704. [[CrossRef](#)] [[PubMed](#)]
49. Yuantao, L.; Bing, C.; Zhaohui, Q.; Dong, P.; Aminul Haque, M. Experimental research on properties and microstructures of magnesium-iron phosphate cement. *Constr. Build. Mater.* **2020**, *257*. [[CrossRef](#)]
50. Qoku, E.; Scheibel, M.; Bier, T.; Gerz, A. Phase development of different magnesium phosphate cements at room temperature and elevated temperatures. *Constr. Build. Mater.* **2021**, *272*, 121654. [[CrossRef](#)]
51. Lee, S.-H.; Yoo, B.-H.; Lim, S.J.; Kim, T.-H.; Kim, S.-K.; Kim, J.Y. Development and validation of an equilibrium model for struvite formation with calcium co-precipitation. *J. Cryst. Growth* **2013**, *372*, 129–137. [[CrossRef](#)]
52. Kannan, S.; Ventura, J.M.G.; Lemos, A.F.; Barba, A.; Ferreira, J.M.F. Effect of sodium addition on the preparation of hydroxyapatites and biphasic ceramics. *Ceram. Int.* **2008**, *34*, 7–13. [[CrossRef](#)]
53. El-dek, S.I.; Mansour, S.F.; Ahmed, M.A.; Ahmed, M.K. Microstructural features of flower like Fe brushite. *Prog. Nat. Sci.* **2017**, *27*, 520–526. [[CrossRef](#)]

54. El Hazzat, M.; El Hamidi, A.; Halim, M.; Arsalane, S. Complex evolution of phase during the thermal investigation of Brushite-type calcium phosphate  $\text{CaHPO}_4 \cdot 2\text{H}_2\text{O}$ . *Materialia* **2021**. [[CrossRef](#)]
55. Perwitasari, D.S.; Muryanto, S.; Jamari, J.; Bayuseno, A.P. Kinetics and morphology analysis of struvite precipitated from aqueous solution under the influence of heavy metals:  $\text{Cu}^{2+}$ ,  $\text{Pb}^{2+}$ ,  $\text{Zn}^{2+}$ . *J. Environ. Chem. Eng.* **2018**, *6*, 37–43. [[CrossRef](#)]
56. Karbakhshravari, M.; Abeysiriwardana-Arachchige, I.S.A.; Henkanatte-Gedera, S.M.; Cheng, F.; Papelis, C.; Brewer, C.E.; Nirmalakhandan, N. Recovery of struvite from hydrothermally processed algal biomass cultivated in urban wastewaters. *Resour. Conserv. Recy.* **2020**, *163*, 105089. [[CrossRef](#)]
57. Bayuseno, A.P.; Perwitasari, D.A.; Muryanto, S.; Tauviqirrahman, M.; Jamari, J. Kinetics and morphological characteristics of struvite ( $\text{MgNH}_4\text{PO}_4 \cdot 6\text{H}_2\text{O}$ ) under the influence of maleic acid. *Heliyon* **2020**, *6*, 03533. [[CrossRef](#)] [[PubMed](#)]
58. Huang, H.; Lia, J.; Li, B.; Zhang, D.; Zhao, N.; Tang, S. Comparison of different K-struvite crystallization processes for simultaneous potassium and phosphate recovery from source-separated urine. *Sci. Total Environ.* **2019**, *651*, 787–795. [[CrossRef](#)]
59. Alshaaer, M.; Cuypers, H.; Rahier, H.; Wastiels, J. Production of monetite-based Inorganic Phosphate Cement (M-IPC) using hydrothermal post curing (HTPC). *Cem. Concr. Res.* **2011**, *41*, 30–37. [[CrossRef](#)]
60. Gashti, M.P.; Stir, M.; Jurg, H. Growth of strontium hydrogen phosphate/gelatin composites: A biomimetic approach. *New J. Chem.* **2016**, *40*, 5495–5500. [[CrossRef](#)]
61. Tortet, L.; Gavarrri, J.R.; Nihoul, G. Study of Protonic Mobility in  $\text{CaHPO}_4 \cdot 2\text{H}_2\text{O}$  (Brushite) and  $\text{CaHPO}_4$  (Monetite) by Infrared Spectroscopy and Neutron Scattering. *J. Solid State Chem.* **1997**, *132*, 6–16. [[CrossRef](#)]
62. Dosen, A.; Giese, R.F. Thermal decomposition of brushite,  $\text{CaHPO}_4 \cdot 2\text{H}_2\text{O}$  to monetite  $\text{CaHPO}_4$  and the formation of an amorphous phase. *Am. Mineral.* **2011**, *96*, 368–373. [[CrossRef](#)]
63. Kannan, S.; Lemos, I.A.F.; Rocha, J.H.G.; Ferreira, J.M.F. Synthesis and characterization of magnesium substituted biphasic mixtures of controlled hydroxyapatite/b-tricalcium phosphate ratios. *J. Solid State Chem.* **2005**, *178*, 3190–3196. [[CrossRef](#)]
64. Frost, R.L.; Palmer, S.J. Thermal stability of the ‘cave’ mineral brushite  $\text{CaHPO}_4 \cdot 2\text{H}_2\text{O}$ —Mechanism of formation and decomposition. *Thermochim. Acta* **2011**, *521*, 14–17. [[CrossRef](#)]
65. Hövelmann, J.; Stawski, T.M.; Besselink, R.; Freeman, H.M.; Dietmann, K.M.; Mayanna, S.; Pauw, B.R.; Benning, L.G. A template-free and low temperature method for the synthesis of mesoporous magnesium phosphate with uniform pore structure and high surface area. *Nanoscale* **2019**, *11*, 6939–6951. [[CrossRef](#)] [[PubMed](#)]
66. Prywer, J.; Sieroń, L.; Czyłkowska, A. Struvite Grown in Gel, Its Crystal Structure at 90 K and Thermoanalytical Study. *Crystals* **2019**, *9*, 89. [[CrossRef](#)]
67. Wang, C.; Hao, X. Small-Scale Formation of Struvite by Electrochemical Deposition and Its Characterization. In Proceedings of the 3rd International Conference on Bioinformatics and Biomedical Engineering, Beijing, China, 11–13 June 2009; pp. 1–4. [[CrossRef](#)]
68. Alshaaer, M.; Abdel-Fattah, E.; Saadeddin, I.; Al Battah, F.; Issa, K.I.; Saffarini, G. The effect of natural fibres template on the chemical and structural properties of Biphasic Calcium Phosphate scaffold. *Mater. Res. Express* **2020**, *7*, 065405. [[CrossRef](#)]
69. Alshaaer, M.; Afify, A.S.; Moustapha, M.E.; Hamad, N.; Hammouda, G.A.; Rocha, F. Effect of full-scale substitution of strontium for calcium on the microstructure of brushite:  $(\text{Ca}_x\text{Sr}_{1-x})\text{HPO}_4 \cdot n\text{H}_2\text{O}$  System. *Clay Miner.* **2021**. [[CrossRef](#)]
70. Ding, H.; Pan, H.; Xu, X.; Tang, R. Toward a Detailed Understanding of Magnesium Ions on Hydroxyapatite Crystallization Inhibition. *Cryst. Growth Des.* **2014**, *14*, 763–769. [[CrossRef](#)]
71. Nielsen, M.R.; Sand, K.K.; Rodriguez-Blanco, J.D.; Bovet, N.; Generosi, J.; Dalby, K.N.; Stipp, S.L.S. Inhibition of Calcite Growth: Combined Effects of  $\text{Mg}^{2+}$  and  $\text{SO}_4^{2-}$ . *Cryst. Growth Des.* **2016**, *16*, 6199–6207. [[CrossRef](#)]
72. Muhammed, M.; Mujeeb, R.; Surya, R.D.; Rekha, P. Investigation on growth and morphology of in vitro generated struvite crystals. *Biocatal. Agric. Biotechnol.* **2019**, *17*, 566–570. [[CrossRef](#)]